THE JOURNAL OF BIOLOGICAL CHEMISTRY VOL. 290, NO. 10, pp. 6203–6214, March 6, 2015

Tyrosyl-DNA Phosphodiesterase I Catalytic Mutants Reveal an Alternative Nucleophile That Can Catalyze Substrate Cleavage*

Received for publication, December 24, 2014, and in revised form, January 20, 2015 Published, JBC Papers in Press, January 21, 2015, DOI 10.1074/jbc.M114.635284

Evan Q. Comeaux[‡], Selma M. Cuya[‡], Kyoko Kojima[§], Nauzanene Jafari[¶], Keith C. Wanzeck[‡1], James A. Mobley[‖], Mary-Ann Bjornsti[‡], and Robert C. A. M. van Waardenburg[‡2]

From the [‡]Department of Pharmacology and Toxicology, University of Alabama at Birmingham, Birmingham, Alabama 35294, the [§]University of Alabama at Birmingham Comprehensive Cancer Center, University of Alabama at Birmingham, Birmingham, Alabama 35294, [¶]Department of Molecular Pharmacology, St. Jude Children's Research Hospital, Memphis, Tennessee 38105, and the [‖]Department of Surgery, University of Alabama at Birmingham, Birmingham, Alabama 35294

Background: Tdp1 repair of adducted DNA involves a covalent enzyme-DNA intermediate, formed and resolved by His^{nuc} and His^{gab} residues. Stabilized His^{gab} mutant-DNA complexes are cytotoxic.
Results: DNA adduct cleavage by an adjacent His residue in His^{nuc}Ala mutants impair enzyme-DNA intermediate resolution.
Conclusion: Alterations in active site geometry enhance the stability of cytotoxic Tdp1-DNA intermediates.
Significance: These findings provide the rationale for developing chemotherapeutics that poison Tdp1.

Tyrosyl-DNA phosphodiesterase I (Tdp1) catalyzes the repair of 3′-DNA adducts, such as the 3′-phosphotyrosyl linkage of DNA topoisomerase I to DNA. Tdp1 contains two conserved catalytic histidines: a nucleophilic His (His^{nuc}) that attacks DNA adducts to form a covalent 3′-phosphohistidyl intermediate and a general acid/base His (His^{gab}), which resolves the Tdp1-DNA linkage. A His^{nuc} to Ala mutant protein is reportedly inactive, whereas the autosomal recessive neurodegenerative disease SCAN1 has been attributed to the enhanced stability of the Tdp1-DNA intermediate induced by mutation of His^{gab} to Arg. However, here we report that expression of the yeast His^{nuc}Ala (H182A) mutant actually induced topoisomerase I-dependent cytotoxicity and further enhanced the cytotoxicity of Tdp1 His^{gab} mutants, including H432N and the SCAN1-related H432R. Moreover, the His^{nuc}Ala mutant was catalytically active *in vitro*, albeit at levels 85-fold less than that observed with wild type Tdp1. In contrast, the His^{nuc}Phe mutant was catalytically inactive and suppressed His^{gab} mutant-induced toxicity. These data suggest that the activity of another nucleophile when His^{nuc} is replaced with residues containing a small side chain (Ala, Asn, and Gln), but not with a bulky side chain. Indeed, genetic, biochemical, and mass spectrometry analyses show that a highly conserved His, immediately N-terminal to His^{nuc}, can act as a nucleophile to catalyze the formation of a covalent Tdp1-DNA intermediate. These findings suggest that the flexibility of Tdp1 active site residues may impair the resolution of mutant Tdp1 covalent phosphohistidyl intermediates and provide the rationale for developing chemotherapeutics that stabilize the covalent Tdp1-DNA intermediate.

Tyrosyl-DNA phosphodiesterase I (Tdp1)[3] is a eukaryotic DNA repair enzyme that can remove a wide variety of 3′-phospho-DNA adducts. The 3′-phosphotyrosyl linkage of DNA topoisomerase I (Top1) to a single DNA end was first identified as a Tdp1 substrate (1). The covalent enzyme-DNA complex is a requisite intermediate in the catalytic cycle of Top1 and constitutes the sole cellular target of the camptothecin (CPT) class of cancer therapeutics. CPTs, which include the Food and Drug Administration-approved analogs topotecan and irinotecan, reversibly stabilize the covalent Top1-DNA complex to induce S phase-specific lethal DNA lesions (2–6). More recently, Tdp1 has been shown to process a wide range of other DNA adducts, including 3′-modified nucleotides, such as phosphoglycolates and chain-terminating nucleotides, and a 3′-phosphohistidyl intermediate formed during Tdp1 catalysis (7–13).

As a member of the phospholipase D superfamily, Tdp1 contains conserved histidine-lysine motifs (H*X*K) that provide the two catalytic histidine residues for hydrolysis of its substrates (see Fig. 1*A*) (14–17). The more N-terminal catalytic histidine (herein referred to as His^{nuc}, which is His^{182} in yeast and His^{263} human Tdp1) functions in the nucleophilic attack on the 3′-phosphoryl-adduct linkage to form a 3′-phosphohistidyl bond between Tdp1 and DNA. A more C-terminal catalytic histidine (referred to as His^{gab}, which in yeast is His^{432} and in human His^{493}) then functions as a general acid/base to activate a water molecule to hydrolyze the Tdp1-DNA linkage, dissociating Tdp1 from the DNA (see Fig. 1*B*). Tdp1 leaves behind a

* This work was supported, in whole or in part, by National Institutes of Health Grant CA58755 (to M. A. B.) and NCI Grant 5P30CA013148. This work was also supported in part by funds from the Alabama Drug Discovery Alliance (to R. C. A. M. v. W.) and a Comprehensive Cancer Center Core Support Grant (to A. M. and K. K.).

[1] Present address: Dept. of Medicine, Division of Clinical Immunology & Rheumatology, University of Alabama at Birmingham, Birmingham, AL 35294.
[2] To whom correspondence should be addressed: Dept. of Pharmacology and Toxicology, VH 155, 1720 2nd Ave. S., University of Alabama at Birmingham, Birmingham, AL 35294-0019. Tel.: 205-934-4572; Fax: 205-934-8240; E-mail: rvanwaar@uab.edu.

[3] The abbreviations used are: Tdp1, Tyrosyl-DNA phosphodiesterase I; Top1, DNA Topoisomerase I; CPT, camptothecin; SCAN1, Spinocerebellar ataxia with axonal neuropathy; His^{nuc}, nucleophilic histidine; His^{gab}, general acid/base histidine; nLC-ESI-MS(MS), nano-HPLC electrospray ionization multistage tandem mass spectrometry.

DNA nick with 3′-phosphoryl and 5′-OH ends, which must be processed by polynucleotide kinase/phosphatase for DNA ligation (18–21). The catalytic mechanism of Tdp1 and catalytic pocket architecture are highly conserved between yeast and human Tdp1 (see Fig. 1, *A* and *B*) (7, 12, 15–17, 22, 23).

A catalytic His^{gab} to Arg substitution in human Tdp1 (H493R) was identified in patients with the rare autosomal recessive neurodegenerative disease spinocerebellar ataxia with axonal neuropathy (SCAN1) (13). Replacing His^{gab} with Arg impairs the resolution of the Tdp1-DNA phosphohistidyl linkage, resulting in a longer-lived covalent Tdp1-DNA reaction intermediate *in vitro* (10, 23). Consequently, SCAN1 lymphoblastoid cells or yeast cells expressing the analogous yeast His^{gab} to Arg (H432R) mutant are more sensitive to CPT-induced DNA lesions or to oxidative DNA damage induced by H_2O_2, γ-irradiation, or bleomycin (7, 23–25). However, in patients, the SCAN1 phenotype is not evident until the second decade of life, is restricted primarily to the neurodegeneration of cerebellar neurons, and is not associated with an increased risk of cancer or immune deficiency (13). Thus, the defect in Tdp1 catalysis imparted by the H432R mutation does not suffice to induce acute cellular toxicity; rather it is likely that the cumulative effects of chronic Tdp1-DNA stabilization induce the neuropathology of SCAN1.

In structural studies of the analogous SCAN1-like mutation in yeast Tdp1 (H432R), crystallographic data revealed a more shallow catalytic pocket with increased positive charge, in comparison with wild type Tdp1 (23). Such alterations in electrostatic potential appear to enhance the noncovalent binding of Tdp1 to DNA. Yet this increment in substrate affinity fails to explain the defect in (H432R) SCAN1 mutant catalysis. For example, a similar change in electrostatic potential and DNA binding was induced in the H432K mutant; however, this substitution did not impair the resolution of the covalent Tdp1-DNA linkage. Indeed, the catalytic activity of this mutant is similar to that of wild type Tdp1 (23). In contrast, substitution of His^{gab} with residues that contain smaller polar or aliphatic side chains (including Asn, Glu, Leu, Ala, Ser, or Thr) induces an even more severe lethal phenotype, effectively transforming Tdp1 into a potent Top1-dependent cellular toxin, even in the absence of CPT (7, 23).

To investigate how seemingly subtle alterations in His^{gab} have profoundly distinct effects on cell viability, we focused on the coordinated function of His^{gab} with His^{nuc} during mutant Tdp1 catalysis (see Fig. 1*A*). For example, mutation of the His^{nuc} to Ala in human and yeast Tdp1 has been reported to inhibit Tdp1 catalytic activity in in vitro assays (12, 16, 26, 27). We therefore hypothesized that introducing the His^{nuc}Ala mutation into the His^{gab} mutant proteins would suppress the enhanced CPT sensitivity of the SCAN1 H432R mutant and the Top1-dependent lethality of the more toxic H432N mutant (7, 23, 24). Surprisingly, however, we report here that the His^{nuc}Ala substitution (H182A) actually potentiated the cytotoxicity of the His^{gab} mutants and induced a Top1-independent lethal phenotype in combination with the H432N mutant. In contrast, the introduction of a bulky Phe residue at residue 182 completely suppressed the catalytic activity and the toxicity of the His^{gab} mutants. Our findings suggest that in the H182A mutant, a conserved His^{181} residue provides an alternative nucleophile for substrate hydrolysis, an activity that is constrained by the active site geometry of wild type Tdp1 or the H182F mutant. Moreover, the enhanced flexibility of H182A active site residues appears to impair the resolution of mutant His^{gab} covalent phosphohistidyl intermediates. These results are discussed in terms of the catalytic mechanism of Tdp1 and provide the rationale for developing chemotherapeutics that stabilize rather than inhibit the formation of the covalent Tdp1-DNA intermediate.

EXPERIMENTAL PROCEDURES

Yeast Strains, Plasmids, and Drugs—DMSO and CPT were obtained from Sigma. *Saccharomyces cerevisiae* strain KWY3 [*top1*Δ, *TDP1*] (*MATα, ura3*Δ::*LoxP his3*Δ*200 leu2*Δ*1 trp1*Δ*63 top1*Δ::*HIS5*) was generated from FY-250 (*MATα, ura3-52, his3A200, leu2Al, trp1*Δ*63*) by gene replacement of *TOP1* with *HIS5* and the *ura3-52* allele with LoxP-KAN^r-LoxP, followed by Cre-mediated recombination to yield *ura3*Δ::*LoxP* (28, 29). KWY4 [*top1*Δ,*tdp1*Δ] (*MATα, ura3*Δ::*LoxP his3*Δ*200 leu2*Δ*1 trp1*Δ*63 tdp1*Δ *top1*::*HIS5*) was generated from KWY3 via deletion of *TDP1* using *URA3* flanked by gene endogenous 3′-UTR repeats, followed by selection on 5-fluoroorotic acid (23, 30). ECY3 [*MMY3, tdp1*Δ::*URA3*] and ECY4 [*MMY4, tdp1*Δ::*URA3*] were generated from MMY3 (*MATα, ura3-52 his3*Δ*200 leu2*Δ*1 trp*Δ*63 top1*Δ::*TRP1 rad9*::*hisG*) and MMY4 (*MATα, ura3-52 his3*Δ*200 leu2*Δ*1 trp1*Δ*63 rad9*::*hisG*) (31) by gene replacement of *TDP1* with *URA3*, respectively. ECY2 (KWY4, *pep4*Δ::*TRP1, prb1*Δ::*URA3*) was generated by gene replacement of *PEP4* with *TRP1* and *PRB1* with *URA3* in KWY4. In all cases, gene deletions were confirmed by PCR and DNA sequencing.

For cell viability studies, the *tdp1* alleles were expressed from the galactose-inducible promoter *GAL1* in YCpGAL1TDP1·L vectors as described in Gajewski *et al.* (23). *tdp1* mutant alleles were created using QuikChange Site-Directed Mutagenesis kit (Stratagene). yTop1 was constitutively expressed at elevated levels from the *GPD* promoter YCpGDP-TOP1·U (28). The yTop1Y727F catalytic inactive mutant was expressed from the galactose-inducible *GAL1* promoter of the YCpGAL1-Top1Y727F·U plasmids (7, 31). For protein purification from yeast, we first introduced *GAL4* coding sequences downstream of the bidirectional *10GAL1* promoter in YEpGAL4–10GAL1·L to enhance galactose-induced expression from the GAL1 promoter. N-terminal Flag-tagged *tdp1* constructs, produced by PCR amplification, were subsequently cloned into this vector to yield YEpGAL4–10GAL1-tdp1·L vectors. All *TDP1* alleles were confirmed by DNA sequencing. PCR primer sequences are available upon request.

Immunoblotting of Yeast Cell Extracts—Anti-yeast Tdp1 antibodies were previously described (7) and anti-tubulin antibodies (MCA77G) were from AbD Serotec. Briefly, as described (7), cultures expressing Tdp1 from YCpGAL1 constructs were induced for 6 h with 2% galactose, corrected to the same A_{595} and lysed by vortexing with acid-washed glass beads at 4 °C in 50 mM Tris, pH 8.0, 2 mM EDTA, 2 mM EGTA, 10% glycerol, and Complete EDTA-free protease inhibitor (Roche). Proteins were resolved on a 12% SDS-PAGE, blotted onto PVDF, immunostained with anti-Tdp1 and anti-tubulin antibodies, and visualized by chemiluminescence.

Yeast Cell Viability Assays—Semi-quantitative colony formation assays were performed as described in He *et al.* (7). Briefly, cultures of yeast cells, co-transformed with indicated vectors, were diluted to $A_{595} = 0.3$ in TE buffer (50 mM Tris, pH 8.0, 5 mM EDTA) and serially diluted 10-fold. Aliquots (5 μl) were then spotted onto selective media plates containing 2% galactose, with or without the indicated concentration of CPT, 0.0025% DMSO, and 25 mM HEPES, pH 7.2, and incubated for 4 days at 30 °C. At least three independent experiments were performed.

Quantitative colony formation assays were also performed, as described in Ref. 23. Briefly, exponential cultures of cells transformed with the indicated vectors were corrected to $A_{595} = 0.3$, 10-fold serially diluted, and plated on selective medium containing 2% galactose. The number of viable cells forming colonies were counted following incubation at 30 °C. All experiments ($n \geq 3$) were performed in duplicate.

Purification of Tdp1 Proteins—N-terminal Flag-tagged yeast Tdp1 proteins were expressed from YEpGAL4–10GAL1-tdp1·L vectors in protease-deficient *tdp1*Δ, *top1*Δ cells (strain ECY2). Exponential cultures were induced with 2% galactose for 6 h, cells were harvested, and Tdp1 proteins were purified as described (23). Briefly, cell extracts in HEE buffer (50 mM HEPES, pH 8.0, 5 mM EDTA, 5 mM EGTA) were loaded onto SP-Sepharose fast flow matrix (GE Life Sciences), eluted with HEE and 0.4 M NaCl, and then affinity-purified by anti-Flag M2 (Sigma) affinity matrix chromatography. Flag-Tdp1 was eluted with 3× Flag peptide in TEEK (50 mM Tris, pH 7.5, 1 mM EDTA, 1 mM EGTA, 100 mM KCl, 1 mM DTT) and was concentrated in an Ultracel-30K concentrator (Millipore). Protein purity was determined by SYPRO Ruby (Bio-Rad) staining of Tdp1 fractions resolved by 12% SDS-PAGE.

Tdp1 in Vitro Activity Assays—Tdp1 activity was assessed as described (23). Briefly, a 14-mer (5′-GATCTAAAAGACTT-3′) oligonucleotide with a 3′-phosphotyrosine was used as substrate, and an identical oligonucleotide with a 3′-phosphate served as substrate control (Midland Certified Reagent Company, Inc.). 5′-^{32}P end-labeled oligonucleotide, 16.7 nM under unsaturated conditions, and 1000 nM for saturated conditions was incubated in reaction buffer (50 mM Tris, pH 7.5, 2 mM EDTA, 100 mM KCl, 2 mM DTT) with the indicated amounts of Tdp1. After 10 min at 30 °C, half the sample was combined with USB stop buffer and 8 M urea for analysis in 20% polyacrylamide/urea sequencing gels, whereas the other half was subjected to 12% SDS-PAGE. To determine enzyme kinetics of wild type Tdp1 and the H182A, H432R, and H432N mutant enzymes, we used the same reaction conditions as described above but at one enzyme concentration (that converts 40% or less substrate to product) and increasing concentrations of substrate. Reaction products were visualized by phosphorimaging analysis and quantified with ImageQuant TL 1D version 7.0 (GE Healthcare). Product concentrations and initial velocity were calculated from the ratio of the integrated intensities of substrate and product (which is equal to enzyme-DNA intermediate + 3′-phosphoryl product) bands. Four independent reactions were analyzed using nonlinear regression fitting of the Michealis-Menten equation to calculate the K_m and V_{max} values with the VisualEnzymics software (Soft Zymics, Inc., Charlottesville, VA) in the IGOR PRO 6 program 2010 (WaveMetrics, Portland, OR).

nLC-ESI-MS(MS)—In vitro reactions, prepared with 2 μg of Tdp1H182A with or without oligonucleotide (as above), were incubated with 3000 units of micrococcal nuclease at 37 °C for 30 min, then resolved by 4–12% SDS Bis-Tris PAGE, and stained with colloidal blue (Invitrogen). α-Casein (5 μg) was included as both a carrier protein and as an internal quality control. For in gel digestion, bands corresponding to ~70 kDa (Tdp1) and 19–25 kDa (α-casein) were excised, equilibrated in 100 mM ammonium bicarbonate, reduced with 10 mM DTT, carbidomethylated with 55 mM iodoacetamide, dehydrated, and digested with Trypsin Gold (Promega). The digested peptides were concentrated under vacuum, resolubilized in 0.1% formic acid, and injected onto a Surveyor HPLC plus (Thermo Scientific) using a split flow configuration on the back end of a 100-micron-inner diameter × 13-cm pulled tip C-18 column (Jupiter C-18 300 Å, 5 microns; Phenomenex). Peptide fractions were then directly sprayed into a Thermo Orbitrap Velos Pro hybrid mass spectrometer equipped with a nano-electrospray source over a 1-h gradient set to increase from 0–30% acetonitrile in deionized H_2O containing 0.1% formic acid with a flow rate of 0.3 μl/min. Following each parent ion scan, fragmentation data were collected on the top most intense 15 ions, in collision-induced dissociation mode, with the following instrument settings: spray voltage, 1.9 kV; capillary temperature, 170 °C; and 1 microscan, with the scan window set at 300–2,00 m/z, and maximum inject times of 500 and 100 ms for the parent ion and fragmentation scans, respectively. The parent ion scans were obtained at 60 K resolution in the Oritrap with a minimum signal threshold of 2000 counts. The activation settings were: charge state, +2; isolation width, 2.0; m/z, normalized collision energy, 35.0; activation Q, 0.250; and activation time, 25 ms. For data-dependent settings, monoisotopic precursor selection was enabled, in addition to charge state screening with rejection of 1+ ions, and dynamic exclusion with repeat count of 2, repeat duration of 30 s, exclusion list size of 500, and exclusion duration of 90 s.

The XCalibur RAW files collected in profile mode were centroided and converted to MzXML using ReADW v. 3.5.1. The .mgf files were created using MzXML2Search for all scans with a precursor mass between 300 and 2,000 Da. The data were searched using SEQUEST set for three maximum missed cleavages, a precursor mass window of 20 ppm, trypsin digestion, and variable modification C at 57.0293 and M at 15.9949. For the fragment-ion mass tolerance, 0.0 Da was used. Searches were performed with the SGD database with protein sequences specific to these experiments included, and peptide IDs were filtered using Scaffold (Proteome software), with cutoff values set with peptide length (>5 amino acids) and excluding peptides with a MH+1 charge state. Peptide probabilities were set to >90% C.I., with the number of peptides/protein set at 2 or more and protein probabilities set to >97% confidence interval, resulting in protein IDs with >99% confidence. Two-dimensional time and mass plots were generated in Refiner MS (Genedata, Expressionist).

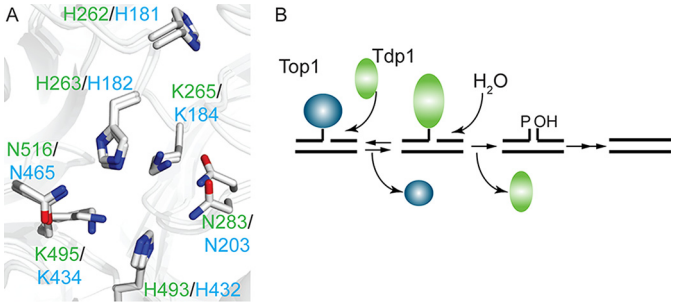

FIGURE 1. **Tdp1 conserved catalytic pocket architecture and mechanism.** *A*, overlay of the crystal structure of yeast and human Tdp1 active site residues that comprise the H*XKX*$_n$N motifs. Human Tdp1 residues are labeled in *green* (Protein Data Bank code 1NOP) (22), and yeast Tdp1 is labeled in *cyan* (Protein Data Bank code 1Q32) (7). His$^{263/182}$ functions as a nucleophile (His^{nuc}), whereas His$^{493/432}$ acts as a general acid-base (His^{gab}). *B*, the two-step Tdp1 catalytic cycle. In step 1, Tdp1 hydrolysis of the Top1-DNA covalent complex by nucleophilic attack of His^{nuc} on the 3′-phosphotyrosyl linkage, forming a 3′-phosphohistidyl bond (Tdp1His^{nuc}-DNA covalent complex). In step 2, water is activated by the general acid/base histidine, His^{gab}, to hydrolyze the Tdp1-DNA linkage, dissociating Tdp1 from the nicked DNA strand. The single-strand break ends need subsequent processing by polynucleotide kinase/phosphatase and DNA ligase to produce intact DNA.

RESULTS

Expression of Tdp1H182A Induces Top1-dependent Toxicity—To study the cellular consequences of Tdp1 catalytic dysregulation, we used the yeast *S. cerevisiae* in which the *TOP1* and *TDP1* genes were deleted (*top1*Δ, *tdp1*Δ) in an otherwise DNA damage response and repair-proficient background (7, 23). Mutant *tdp1* alleles were then expressed from plasmid-borne, galactose-inducible (*GAL1*) promoted constructs to prevent adaptation to cytotoxic mutant enzymes. These studies were also facilitated by elevated Top1 expression to increase cellular levels of the Tdp1 substrate, covalent Top1-DNA covalent complexes.

To investigate the mechanism by which His^{gab} substitutions cause increased Top1-dependent toxicity (23), we focused on the role of the His^{nuc} within the first *HXK* motif (Fig. 1*A*). In yeast Tdp1, His^{nuc} is His^{182}, and His^{gab} is His^{432}. Biochemical studies previously reported that mutation of His^{nuc} to Ala resulted in a catalytically inactive enzyme (16, 26). This outcome is logical, because removing the nucleophile that initiates substrate cleavage should suppress Tdp1 catalysis. Thus, we reasoned that combining the H182A mutation with the His^{gab} mutants would suppress the cytotoxic phenotypes induced by defects in the resolution of the phosphohistidyl intermediate. Surprisingly, however, expression of the H182A mutant, either alone or in combination with the SCAN1-like H432R mutant, actually potentiated the Tdp1-induced toxicity associated with elevated Top1 levels (↑ Top1) and enhanced cell sensitivity to CPT (Fig. 2*A* and Table 1). In these experiments, Tdp1 mutants were expressed in a wild type *TOP1* strain, with or without subtoxic CPT concentrations, to verify that the lethal phenotypes were a consequence of increased covalent Top1-DNA complexes and not elevated Top1 protein levels *per se*. In cells deleted for wild type Tdp1 (*tdp1*Δ strains), galactose-induced expression of Tdp1H182A suppressed the growth of cells with increased levels of Top1 protein (↑ Top1) (Fig. 2*A* and Table 1) and enhanced the CPT sensitivity of cells expressing endogenous levels of Top1 (in Fig. 2*A*, compare *TDP1* and *tdp1H182A*

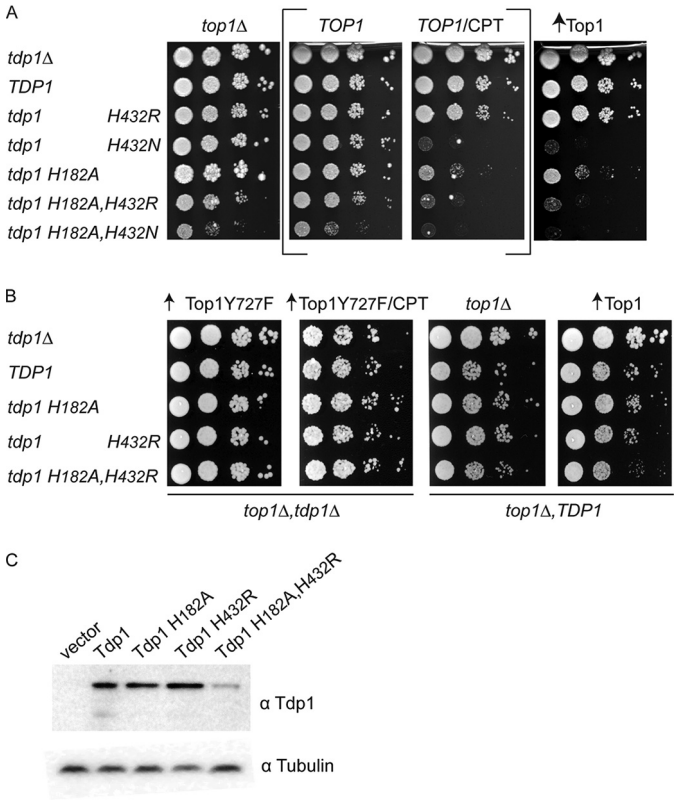

FIGURE 2. **Tdp1H182A induces a substrate-dependent toxicity.** *A*, *top1*Δ,*tdp1*Δ cells were co-transformed with vector control (*top1*Δ) or YCpGPD-Top1·U (↑ Top1) and control vector (*tdp1*Δ) or the indicated YCpGAL1-Tdp1·L, whereas tdp1Δ cells were co-transformed with vector control (*TOP1*) and control vector (*tdp1*Δ) or the indicated YCpGAL1-Tdp1·L. Exponential growing cultures were diluted to A_{595} = 0.3, then 10-fold serially diluted, and spotted onto 2% galactose selective media plates supplemented with or without 1 μg/ml CPT (only for *tdp1*Δ-transformants, shown between *brackets*). *B*, *top1*Δ,*tdp1*Δ cells were transformed with YCpGAL1-Top1Y727F·U (↑ Top1Y727F) and indicated YCpGAL1-Tdp1·L or control vector (*tdp1*Δ), diluted, and spotted (as in *A*) onto selective media plates containing 2% galactose, with or without 5 μg/ml CPT. In addition, *top1*Δ,*TDP1* cells were transformed with vector control (*top1*Δ) or YCpGPD-Top1·U (↑ Top1) and the indicated YCpGAL1-Tdp1·L or vector control (*tdp1*Δ), diluted, and spotted (as in *A*) onto selective media plates containing 2% galactose. All plates were incubated for 4 days at 30 °C. *C*, total cell extracts collected from 6-h galactose-induced *top1*Δ,*tdp1*Δ cells co-transformed with vector control (*top1*Δ), and the indicated YCpGAL1-Tdp1vL or control vector (*tdp1*Δ) used in *A* were resolved on 12% SDS-PAGE and immunoblotted with anti-yeast Tdp1 and anti-α-tubulin.

in the *TOP1/CPT panel*). In the context of the His^{gab} mutants, introducing the H182A substitution into the *H432R* allele induced an even more pronounced Top1-dependent lethal phenotype (Table 1 and Fig. 2*A*, *TOP1/CPT* and ↑ *Top1 panels*), not evident with the single H432R mutant. The results obtained with the H432N mutant were even more surprising. Although expression of the H432N mutant alone induces Top1-dependent toxicity (Fig. 2*A*, *TOP1/CPT* and ↑ *Top1 panels*; Table 1; and Refs. 7 and 23), expression of the double H182A,H432N mutant was toxic even in the absence of Top1 (Fig. 2*A*, *top1*Δ *panel*). These data suggest that the inappropriate processing of endogenous Tdp1 substrates, other than Top1-DNA intermediates, also contributes to the Tdp1 mutant-induced toxicity.

To determine whether Tdp1 mutant-induced lethality required a catalytically active Top1, as was previously shown for H432N

TABLE 1

tdp1 mutant-induced cell lethality

*tdp1*Δ,*top1*Δ cells, transformed with YCpGPD-TOP1·U (↑ Top1) and a YCpGAL1-tdp1·L vector, were plated on selective media plates supplemented with galactose and incubated for 4 days at 30 °C.

tdp1 allele[a]	Number of colonies (relative to *tdp1*Δ control)[b]
*tdp1*Δ	1
TDP1	0.82 ± 0.02
tdp1 H432R	0.67 ± 0.05
tdp1 H432N	0.0001 ± 0.0001
tdp1 H182A	0.19 ± 0.14
tdp1 H182A,H432R	0.006 ± 0.03
tdp1 H182A,H432N	0.001 ± 0.002

[a] The indicated *tdp1* allele was expressed from the GAL1 promoter.
[b] The number of viable cells forming colonies at 30 °C was determined, relative to cells transformed with YCpGAL1·L (*tdp1*Δ control) ($n = 3$, standard deviations are shown).

mutant-induced toxicity (23), the single H182A and double H182A,H432R mutants were expressed in cells with elevated levels of catalytically inactive Top1Y727F (31, 32). Indeed, as seen in Fig. 2*B*, cell viability was maintained, either with or without CPT (compare ↑ Top1Y727F and ↑ Top1Y727F/CPT panels). Moreover, these Top1-dependent lethal phenotypes were not simply a result of mutant Tdp1 overexpression. Lower levels of the H182A,H432R mutant protein produced a more severe phenotype than that induced by higher levels of the single H182A mutant protein (Fig. 2*C*). Together, these data support the concept that the degree of Tdp1-induced toxicity is dependent upon the levels of the Top1-DNA substrate and their conversion to Tdp1-DNA intermediates. To address this possibility, we also expressed these mutants in a wild type Tdp1 strain (*top1*Δ, *TDP1*).

Tdp1 is capable of resolving the 3′-phosphohistidyl bond of the Tdp1-DNA intermediate. Thus, yeast and human Tdp1 His^{gab} mutants (including SCAN1) display a recessive phenotype (7, 13, 23, 24, 33). Indeed, expression of endogenous wild type Tdp1 suppressed the Top1-dependent lethality induced by the H182A or H182A,H432R mutant proteins (Fig. 2, *A* and *B*, compare ↑ *Top1 panel*). These data suggest that the cytotoxic lesion(s) induced by the H182A and H182A,H432R mutant proteins is repaired by wild type Tdp1 and likely involves the formation of a covalent Tdp1-DNA complex. Similar results were obtained with the double H182A,H432N mutant, although in this case, the Top1-independent lethality observed in a *top1*Δ strain was only partially suppressed by wild type Tdp1 (data not shown).

Tdp1H182A Is Catalytically Active in Vitro—Our findings suggest that rather than suppressing Tdp1 catalysis, the H182A mutation actually alters the resolution of the Tdp1-DNA intermediate, possibly in a manner similar to the gain of function imparted by the SCAN1 mutant. To directly address the catalytic activity of the H182A mutant, we purified N-terminal, Flag epitope-tagged Tdp1 proteins from a protease-deficient (*top1*Δ, *tdp1*Δ, *pep4*Δ, *prb1*Δ) yeast strain, as described previously (23). As diagrammed in Fig. 3*A*, the proteins were then incubated in reaction mixtures using a ^{32}P 5′-end-labeled single-stranded 14-mer oligonucleotide modified with a 3′-phosphotyrosyl as substrate (23). Each reaction was then split into two samples and analyzed either for conversion of the 3′-phosphotyrosyl linkage to a 3′-phosphoryl-oligonucleotide product by denaturing 8 M urea, 20% PAGE or for the formation of covalent Tdp1-DNA intermediates by 12% SDS-PAGE as described (23). Consistent with previous results under unsaturated substrate conditions, ~1 nM of wild type Tdp1 protein was sufficient to convert 40% of the 16.7 nM substrate to product, whereas the H432R protein exhibited a ~40-fold reduction in activity compared with wild type (Fig. 3, *B* and *C*). The more toxic mutant, H432N, showed a reduction of ~167-fold (~167 nM enzyme) in catalytic activity *versus* wild type (Fig. 3, *B* and *C*). Yet at the highest enzyme amount (416.7 nM), we generally did not observe full conversion of substrate (Fig. 3*C*). No product was detected in "mock" purified extracts (no Tdp1) (data not shown). The H432R reactions also produced covalent protein-DNA intermediates, resolved as a radiolabeled band near the top of the 8 M urea, 20% polyacrylamide gel, or as a ~70-kDa radiolabeled Tdp1 protein band by SDS-PAGE (Fig. 3, *B* and *D*, *asterisks*). In stark contradiction to earlier reports, but consistent with our yeast data, the H182A protein was also catalytically active, albeit with a specific activity ~85-fold lower than that of wild type Tdp1. However, we failed to detect covalent Tdp1H182A-DNA intermediates at protein concentrations sufficient for quantitative conversion of the substrate to product (the absence of a high molecular weight radiolabeled band with 138.9 nM of H182A in Fig. 3, *B* and *D*). These findings contrast with the results obtained with H432R, where covalent reaction intermediates accumulated prior to reaction products (at 13.9 nM in Fig. 3*B*). Instead, 10–25-fold higher concentrations of protein were required to detect low levels of covalent H182A-DNA complexes by denaturing PAGE and SDS-PAGE (Fig. 3*E*). In similar experiments, a 20-fold molar excess of wild type Tdp1 (over substrate) failed to produce detectable enzyme-DNA intermediates (data not shown).

Mass spectrometry and SDS-PAGE analyses of our H182A protein preparations confirmed that over 90% of the protein was Tdp1H182A. Minor contaminants, including the translation elongation factor EFA-1α (~50 kDa), do not covalently bind DNA and are significantly smaller than the ~70-kDa band detected in Fig. 3*E*. Thus, we think it unlikely that the low levels of protein-DNA intermediates detected with H182A are due to minor protein contaminants. Rather, our data demonstrate the catalytic activity of the H182A mutant protein *in vitro* and suggest that the formation of covalent H182A-DNA intermediates may contribute to the Top1-dependent toxicity observed in yeast.

To define the kinetics of wild type and mutant Tdp1 enzyme activity, an enzyme concentration that converts less than 40% of substrate to product was incubated with increasing concentrations of substrate. The data produced a typical hyperbolic curve in a Michaelis-Menten plot (Fig. 3*F*). Using nonlinear regression fit with the Michaelis-Menten equation, we determined the Michealis-Menten constant (K_m) and V_{max} and calculated k_{cat} and the second order rate constants (K_m/k_{cat}) (Table 2). For all reactions, enzyme-DNA intermediates and 3′-phosphoryl reaction products were defined as products, the concentration of which was then divided by enzyme amount (ng) to allow comparison of the different Tdp1 enzymes. Comparison of K_m values revealed that the single H182A, H432N, and H432R mutant enzymes have a 2–5-fold lower affinity for substrate than wild type Tdp1 (depicted in Fig. 3*F*). These dif-

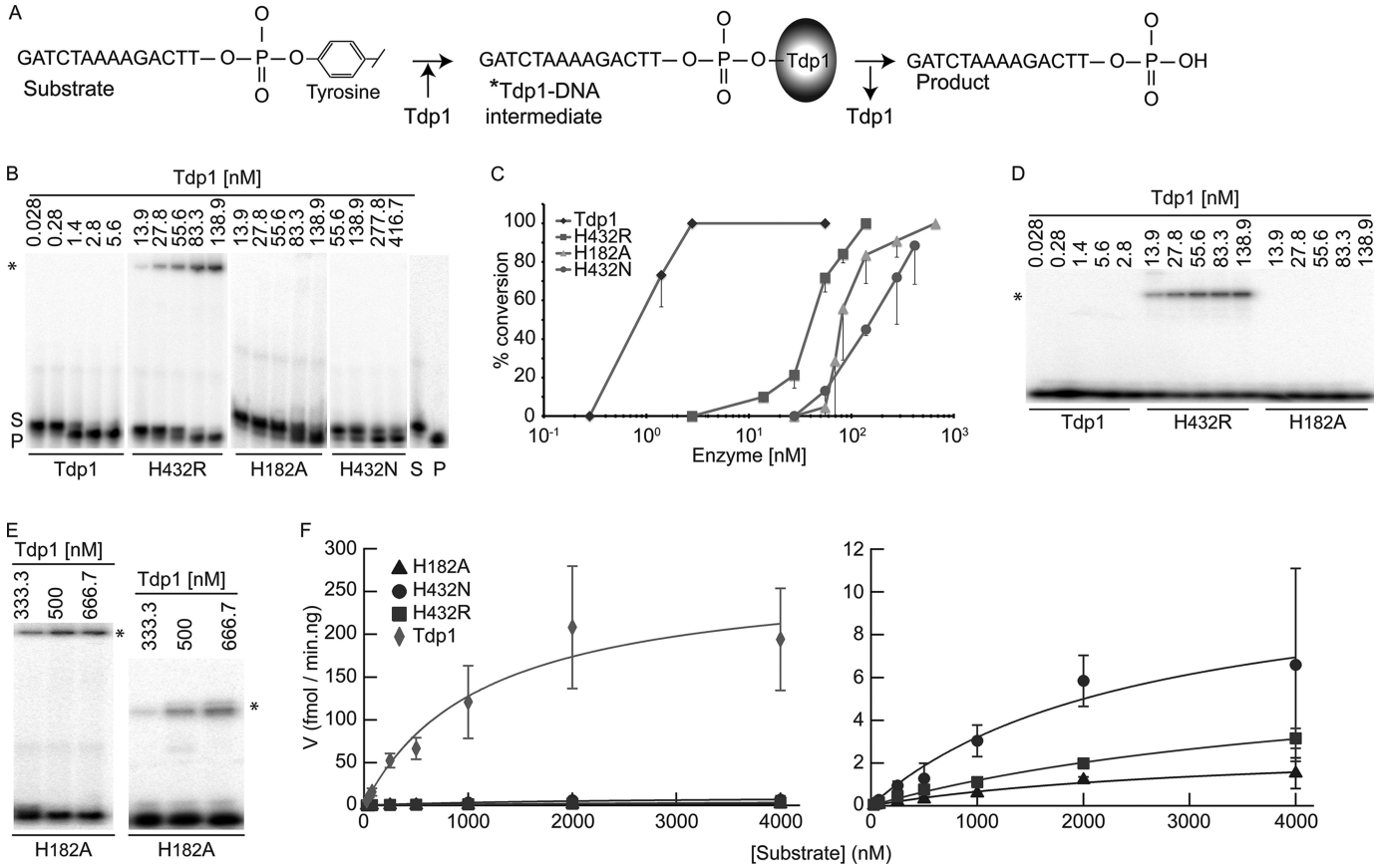

FIGURE 3. **Tdp1H182A is catalytically active.** *A*, schematic of *in vitro* Tdp1 catalytic activity assay. 5′-^{32}P-labeled 14-mer oligonucleotide substrate containing 3′-phosphotyrosine (*Substrate*) is covalently bound by Tdp1 (**Tdp1-DNA intermediate*) and subsequently released as 3′-phosphate (*Product*). *B*, *D*, *E*, and *F*, various concentrations of indicated full-length Tdp1 enzyme were incubated with 16.7 nM (*B*, *D*, and *E*) or 25–4000 nM (*F*) of substrate for 10 min at 30 °C. For *B*, *D*, and *E*, reaction samples were split in two and analyzed as described in *B* and *D* by phosphorimaging. *B*, conversion of 3′-phosphotyrosine (*S*) to 3′-phosphate (*P*) resolved in 20% 8 M urea denaturing polyacrylamide gel. *, covalent Tdp1-DNA intermediates. *C*, the mean and S.D. of the substrate to product (enzyme-DNA intermediate + 3′-phosphoryl product) conversion (product/[product + substrate + intermediate]) from *B* were quantified by phosphorimaging analysis of at least three independent experiments. *D*, detection of covalent protein-DNA reaction intermediates via 12% SDS-PAGE. *E*, reactions with higher concentrations of Tdp1H182A protein analyzed as in *B* (*left panel*) and *D* (*right panel*), respectively. *F*, same reaction conditions as in *B* but with increasing substrate concentrations and constant enzyme concentration. The mean and standard deviation of four independent experiments are shown in a Michaelis-Menten plot (specific velocity (fmol product/min·ng of protein) *versus* [substrate] (nM)) generated with IGOR PRO 6 program 2010. The *right panel* shows an adjusted *y* axis scale from the *left panel* to visualize mutant enzyme results. In *C* and *F*, Tdp1 (*diamond*), H432R (*square*), H182A (*triangle*), and H432N (*circle*).

TABLE 2

Enzyme kinetics

Enzyme kinetics were obtained from four independent experiments, and the kinetic parameters values were determined using nonlinear regression of the Michealis-Menten equation with the VisualEnzymics software in the IGOR PRO 6 program 2010 (shown are averages with standard deviations, $n = 4$).

Enzyme	K_m	V_{max}	k_{cat}	k_{cat}/K_m
	μM	*fmol* $min^{-1} \cdot ng^{-1}$	min^{-1}	$s^{-1} \cdot M^{-1}$
Tdp1	1.1 ± 0.4	273 ± 34	17 ± 2	2.5×10^5
Tdp1H432R	4.8 ± 0.8	6.9 ± 0.7	0.43 ± 0.05	1.5×10^3
Tdp1H432N	2.6 ± 0.8	11.4 ± 1.9	0.7 ± 0.1	4.7×10^3
Tdp1H182A	3.4 ± 0.8	2.9 ± 0.4	0.18 ± 0.03	0.9×10^3

ferences may reflect increased substrate mobility within the larger catalytic pocket of the mutant enzymes, prior to the interactions with active site residues Lys^{184} and Lys^{434}, which allow for His^{nuc} attack of the 3′-phosphotyrosyl linkage. This model is supported by changes in the three-dimensional topology of the catalytic pockets of the mutants *versus* wild type, as revealed in the apo-protein crystal structures (23). However, the relative specific activities of the mutant enzymes (wild type k_{cat} divided by mutant k_{cat}; Table 2) is similar to those obtained with single-turnover experiments for the H432R and H182A mutants, but not the H432N mutant. Even if we compare the second order rate constants (k_{cat}/K_m) of the mutant enzymes with wild type, the H432N mutant still shows the highest relative activity (Table 2). The k_{cat}/K_m value represents how rapidly enzyme turns over under low substrate concentrations. The H432N mutant revealed a higher relative activity (k_{cat} values) under higher substrate conditions (~25-fold less then wild type) than under single-turnover conditions (~170-fold less active then wild type), where substrate is rate-limiting. Yet these relative activities were obtained with a similar enzyme: substrate ratio of ~10 (10-fold more enzyme). These findings suggest that only a fraction of the H432N protein is catalytically active under our near physiological conditions of pH 7.5. Indeed, our modeling of pK_a values of catalytic residues in different Tdp1 mutant enzymes suggested that the His^{nuc} within the H432N mutant catalytic pocket has a high probability to be protonated and therefore catalytically inactive (23).

The Rad9 DNA Damage Checkpoint Suppresses the Top1-dependent Toxicity of Mutant Tdp1—Given the discrepancies between the relatively higher levels of DNA-linked H432R *versus* H182A complexes observed *in vitro*, with the more severe

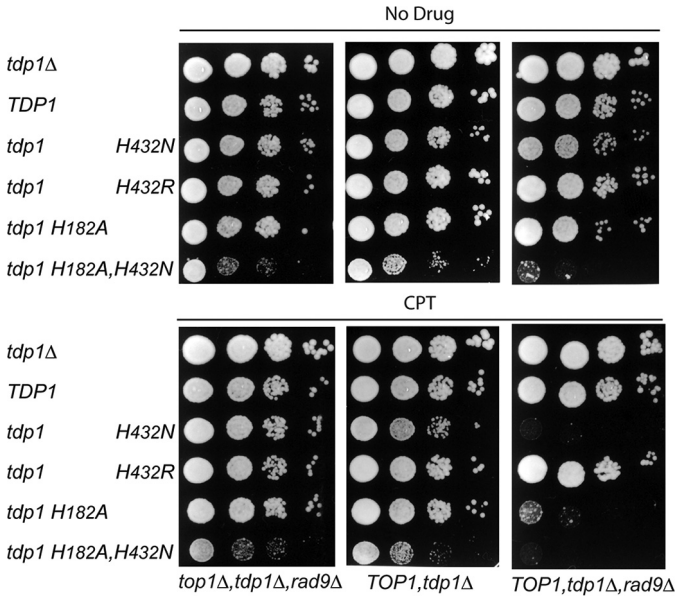

FIGURE 4. **Rad9 DNA damage checkpoint suppresses the Top1-dependent toxicity of mutant Tdp1.** *top1*Δ,*tdp1*Δ,*rad9*Δ, *TOP1*,*tdp1*Δ, and *TOP1*,*tdp1*Δ,*rad9*Δ cells were transformed with the indicated YCpGAL1-Tdp1·L or control vector (*tdp1*Δ) and then 10-fold serially diluted and spotted (as in Fig. *2A*) onto 2% galactose selective media plates supplemented with or without 0.5 μg/ml CPT. The plates were incubated for 4 days at 30 °C.

lethality of the H182A mutants, we next asked whether the Rad9 DNA damage checkpoint could distinguish the cytotoxic lesions induced by the Tdp1 H182A or His^{gab} (H432R or H432N) mutants. Nash and co-workers (26, 34) previously demonstrated that Tdp1 and the homologous recombination protein Rad52 were epistatic in the repair of Top1-DNA cleavable complexes, whereas the Rad9 DNA damage checkpoint proteins functions in a redundant pathway from Tdp1. Indeed, a role for Tdp1 in the repair of Top1 lesions induced by high concentrations of CPT was only evident in yeast cells deleted for the *RAD9* gene (*rad9*Δ) (26, 34–36). Here we asked whether *rad9*Δ would also exacerbate the Top1-dependent lethal phenotypes induced by H182A or the His^{gab} mutants in the absence of drug or in the presence of subtoxic concentrations of CPT. As shown in Fig. 4, in wild type *TOP1* cells, *rad9*Δ had no effect on the viability of cells expressing the single H182A, H432R, or H432N mutants. In the presence of low concentrations of CPT, *rad9*Δ had no impact on the viability of cells expressing wild type Tdp1, no Tdp1 (*tdp1*Δ), or the H432R mutant. In contrast, *rad9*Δ cells expressing H432N or H182A (and Top1) exhibited a 3–4 log increase in CPT sensitivity, relative to isogenic *RAD9* cells. These results implicate a selective role for the Rad9 DNA checkpoint in mediating the repair of H182A- or H432N-induced DNA lesions in the presence of CPT stabilized Top1-DNA complexes, but not in response to increased stabilization of the covalent H432R-DNA intermediate.

The Top1-dependent lethality of the double H182A,H432N mutant was also enhanced in *rad9*Δ cells, even in the absence of CPT (Fig. 4). However, *rad9*Δ had no impact on the Top1-independent toxicity induced by H182A,H432N expression in *top1*Δ cells. The extent of H182A,H432N mutant-induced lethality was indistinguishable between the *top1*Δ,*tdp1*Δ strain shown in Fig. 2*A* and the isogenic *top1*Δ, *tdp1*Δ, *rad9*Δ strain shown in Fig. 4. Thus, whereas the Top1-dependent toxicity elicited by H182A and/or H432N-induced alterations in Tdp1 catalysis appears to involve Rad9-mediated DNA repair, the resolution of Top1-independent lesions induced by the H182A,H432N mutant does not require the Rad9 DNA checkpoint.

The Tdp1H182F Protein Is Catalytically Inactive—The Top1-dependent cytotoxicity of the H182A mutant was surprising, in that this phenotype necessitates the function of a nucleophile, other than His^{182}, in the formation of a Tdp1-DNA intermediate. Given the coordinated activity of the His^{nuc} and His^{gab} residues, and the spatial geometry of these residues in the crystal structures of Tdp1, we next asked whether the smaller side chain of the Ala residue at position 182 was a critical determinant of mutant-induced toxicity, and which residue within the catalytic pocket serves as a nucleophile in the absence of His^{182}. To address these questions, we first generated additional substitutions of His^{182}. Among the mutants generated, we included the polar residues Asn and Gln, because neither can function as a nucleophile yet serve to address whether the size of the side chain at residue 182 is a critical determinant of toxicity. We also mutated His^{182} to Phe to retain the ring structure of the side chain, but without nucleophilic capability. Expression of either the H182N or H182Q mutant induced a similar Top1-dependent toxicity as that observed with the H182A mutant (Fig. 5*A*). However, expression of H182F had no adverse effect on cell viability. Moreover, unlike the H182A,H432R mutant (Fig. 2*A*), combining H182F with the H432R mutant failed to induce a Top1-dependent lethal phenotype (Fig. 5*A*). These data suggest that in contrast to the single H182A, H182N, and H182Q mutants, substitution of His^{182} with Phe results in a catalytically inactive Tdp1 protein.

To directly address this possibility, we purified the H182F mutant protein and assayed enzyme activity using the substrate described in Fig. 3*A*. In reactions containing 5000 fmol of H182F, which represents a 20-fold molar excess of protein over substrate, no conversion of the 3′-phosphotyrosine substrate to a 3′-phosphoryl product was detected (Fig. 5*B*). In contrast, H182A activity was evident at 1250 fmol. These data demonstrate that substitution of the His^{nuc} with Phe suppresses both Tdp1 catalysis and Top1-dependent cellular toxicity.

H182A-induced Toxicity Requires an Adjacent, Conserved His Residue—The observation that H182A possesses some catalytic activity, whereas the H182F mutant is inactive, suggests that the phenolic side chain of Phe prevents the nucleophilic attack on Tdp1 substrates that occurs with a smaller residue at the His^{nuc} position. To ascertain alternative nucleophiles within the Tdp1 active site, we considered the conservation of active site residues in Tdp1 orthologs. As shown in a representative list in Fig. 6*A*, a conserved histidine residue (His^{181} in yeast and His^{262} in human) is immediately N-terminal to the His^{nuc} (Fig. 1*A*) in all but four of 19 known orthologs of Tdp1. To determine whether this conserved adjacent His functions in the formation of a covalent H182A-DNA intermediate, we mutated His^{181} to Ala. Indeed, as seen in Fig. 6*B*, the H181A mutation abolished the Top1-dependent lethality induced by the single H182A and double H182A,H432R and H182A,H432N mutant enzymes (Fig. 6*B* and data not shown). This is probably because these His^{181}

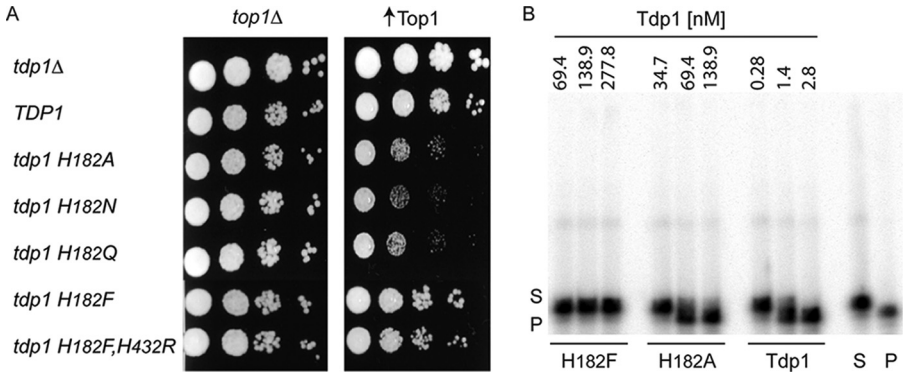

FIGURE 5. **Tdp1H182F protein is catalytically inactive.** *A*, *top1*Δ,*tdp1*Δ cells were transformed with vector control (*top1*Δ) or YCpGPD-Top1·U (↑ Top1) and the indicated YCpGAL1-Tdp1·L or control vector (*tdp1*Δ), 10-fold serially diluted and spotted (as in Fig. *2A*) onto selective media plates with 2% galactose and incubated for 4 days at 30 °C. *B*, *in vitro* Tdp1 catalytic activity assay (as described in Fig. *3A*), with various amounts (fmol) of indicated full-length Tdp1 enzymes resolved in 20% 8 M urea denaturing polyacrylamide gel to detect conversion of 3′-phosphotyrosine (*S*) to 3′-phosphate (*P*).

A

Species	AA#	**H***H* K N
Homo sapiens	251	QAKLDIA-FGT**H***H*TKMMLLLYEEG-LRVVIHTSN
Saccharomyces cerevisiae	170	LIEITMPPFAS**H***H*TKLIINFYDNGECKIFLPSNN
Schizosaccharomyces pombe	108	LYSVYVPMWGT**H***H*SKIMVNFFKDDSCQIVIHTAN
Caenorhabditis elegans	114	VGASLPIPFGT**H***H*TKMSILEDEDGRFHVIVSTAN
Leishmania major	295	LEPPLPVAFGT**Y***H*TKMALCINGKG-LRVSIFTAN
Trypanosoma brucei	108	IKPKLPLPFGV**H***H*GKLILCVNSKG-VRISYLTAN
Xenopus laevis	240	QAKLDIA-YGT**H***H*TKMMLLLYTEG-LRVVIHTSN

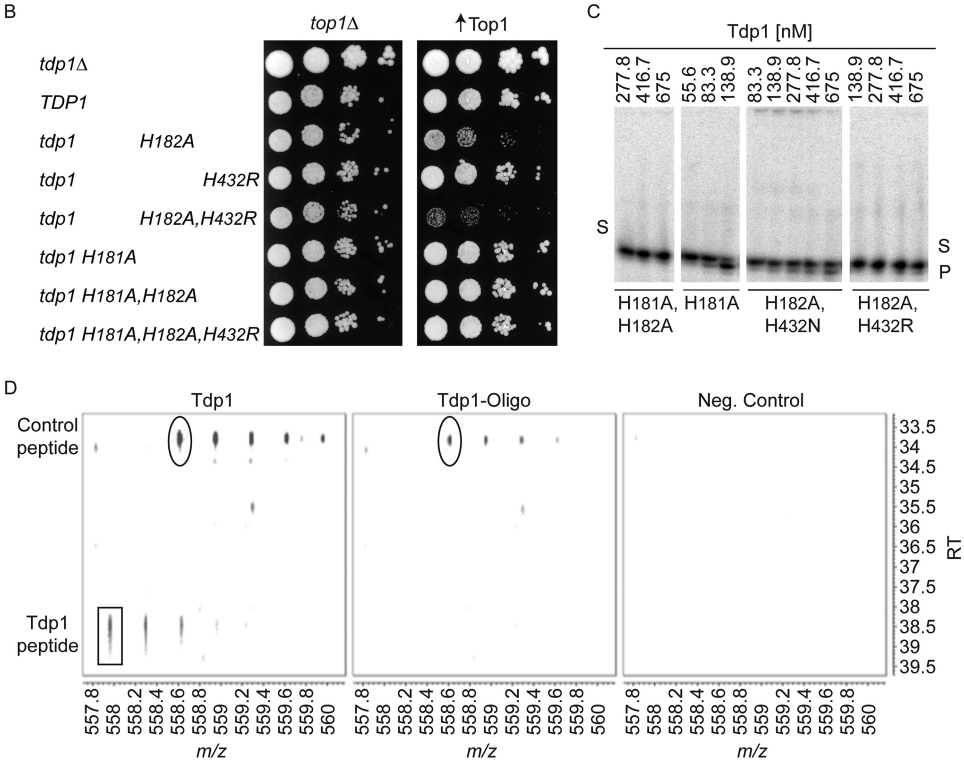

FIGURE 6. **Tdp1H182A toxicity depends on a conserved adjacent histidine residue.** *A*, alignment of a selection of Tdp1 orthologs N-terminal **H***HXKX*$_n$N motif amino acid sequence. The His^{nuc} is italicized, and the adjacent histidine is in bold. *AA#*, amino acid number. UniProt K_D/Swiss-Prot protein numbers were as follows: *Homo sapiens* (Q9NUW8), *S. cerevisiae* (P38319), *Schizosaccharomyces pombe* (Q9USG9), *Caenorhabditis elegans* (Q9TXV7), *Leishmania major* (Q4Q3N1), *Trypanosoma brucei* (Q586D1), and *Xenopus laevis* (Q6DFE8). *B*, *top1*Δ,*tdp1*Δ cells were transformed with vector control (*top1*Δ) or YCpGPD-Top1·U (↑ Top1) and the indicated YCpGAL1-Tdp1·L or control vector (*tdp1*Δ), diluted, and spotted (as in Fig. *2A*) onto selective media plates containing 2% galactose and incubated for 4 days at 30 °C. *C*, conversion of 3′-phosphotyrosine (*S*) to 3′-phosphate (*P*) resolved in 20% 8 M urea denaturing polyacrylamide gel as described for Fig. 3 (*A* and *B*) using 16.7 nM substrate. The mean and standard deviation were determined (graph not shown) as described for Fig. 3*C*, revealing a reduction of relative activity (*versus* wild type enzyme; Fig. 3, *B* and *C*) of ~20-fold for H181A and ~210-fold for H182A,H432N. Relative activity of H182A,H432R could not be determined because it did not convert 50% of substrate. *D*, two-dimensional plot of mass and time tags (557–560 *m/z*, 33–40 min.). The non-cross-linked His^{181}-Ala^{182}-containing tryptic fragment ^{170}LIEITMPPFAS*HA*TK^{184} (Tdp1 peptide, *rectangle*) is illustrated with a mass and time tag of 557.96 *m/z* at 38.3 min (3+ charge state), with good signal intensity in the oligonucleotide-free sample (*Tdp1*) and yet not observed in the oligonucleotide reacted sample (*Tdp1-Oligo*). Serving as a control peptide ^{65}IIDLTNQEQDLSER^{78} (control peptide, *circle*) presented with a similar mass and time tag of 558.62 *m/z* @ 33.7 min (3+ charge state) and was observed at nearly equal intensities in both samples ± oligonucleotide. Neither fragment was observed in the negative control sample (*Neg. Control*).

double and triple mutant proteins are not catalytically active. Indeed, the double H181A,H182A mutant protein did not show any catalytic activity (Fig. 6*C*), suggesting that the triple mutants are also catalytically inactive. Conversely, the single H181A mutant protein is still catalytically active and only ~21-fold less active then wild type Tdp1 (Fig. 6*C* and data not shown). Moreover, the double H182A,H432R and H182A,H432N mutant proteins reveal a dramatic reduction in catalytic activity (Fig. 6*C*). As such, the H182A,H432R enzyme was not able to convert 50% of the substrate at the highest concentration tested (675 nM), whereas the H182A,H432N enzyme revealed a reduction in catalytic activity of ~210-fold (~270 nM enzyme) compared with wild type (Fig. 6*C* and data not shown). This is similar to the single H432N mutant, under conditions where ~200 nM of enzyme converted 50% of the 16.7 nM substrate to product (Figs. 3*B* and 6*C*, compare H432N). This further supports the concept that the loss of a general acid-base residue at position 432 (H432N) increases the probability that the His^{nuc} is protonated to render the enzyme inactive (Fig. 3*B* and Table 2) (23).

To address the ability of His^{181} to function as a nucleophile in a H182A background, we next assessed the formation of a phosphohistidyl bond between His^{181} and the Tdp1 substrate shown in Fig. 3*A*. *In vitro* reactions were performed with 2 μg of purified H182A protein, with or without a nonradioactive substrate, to be analyzed by mass spectrometry. The reaction mixture was first incubated with micrococcal nuclease to remove the bulk of the oligonucleotide substrate, and then the H182A protein was resolved by SDS-PAGE. Protein within the molecular weight range of Tdp1 was recovered from the gel and trypsinized. The resultant peptides were then analyzed by nLC-ESI-MS(MS), with the goal of defining the presence of the His^{181}-Ala^{182}-containing sequence ^{170}LIEITMPPFAS*HA*TK^{184} bound to mononucleotide 3′-T/TCAG. Mass spectrometry analysis revealed similar sequence coverage of Tdp1 in both samples (with or without oligonucleotide). However, whereas the non-cross-linked His^{181}-Ala^{182}-containing fragment (mass and time tag; 557.96 *m*/*z* @ 38.3 min, 3+ charge state) was characterized in the oligonucleotide-free sample with good signal intensity (Fig. 6*D*, *rectangle*), the same tryptic peptide was not observed in the oligonucleotide reacted sample. In contrast, the Tdp1-derived peptide ^{65}IIDLTNQEQDLSER^{78} (mass and time tag; 558.62 *m*/*z* @ 33.7 min, 3+ charge state) was observed at nearly equal intensities in both samples with and without oligonucleotide (Fig. 6*D*, *circle*). Despite several attempts, we were unable to positively characterize the nucleotide-linked amino acid residue by nLC-ESI-MS(MS) analysis, presumably because the mononucleotide modification likely interferes with ionization and fragmentation efficiency. Nevertheless, the comparative analyses of samples obtained with or without oligonucleotide are consistent with the model in which the His^{181}-Ala^{182}-containing tryptic peptide is covalently attached to the mononucleotide via His^{181}.

DISCUSSION

Tdp1 catalyzes the repair of 3′-phospho-DNA adducts and, to a limited extent, 5′-DNA adducts. DNA topoisomerases, on the other hand, catalyze changes in the linkage of DNA strands or helices, whereas site-specific recombinases catalyze the reciprocal exchanges of double-stranded DNA molecules (reviewed in Ref. 37). Yet, despite the biological diversity of these activities, these enzymes share a reaction mechanism that involves the formation of a covalent enzyme-DNA intermediate. In each case, the chemistry of coupled transesterification reactions obviates the need for ATP hydrolysis to effect substrate cleavage or covalent complex resolution. With DNA topoisomerases and site-specific recombinases, a nucleophilic tyrosine or serine initiates the coupled DNA cleavage and religation reactions required to effect changes in DNA topology or DNA recombination. With Tdp1, the coordinated activity of two histidines function in a two-step cycle to remove DNA-phospho-adducts. Moreover, in contrast to the intact DNA strands produced by DNA topoisomerases and recombinases, Tdp1 processing of adducted DNA ends yields a nicked DNA substrate that is subsequently repaired by the concerted action of PNK/DNA ligase (Fig. 1*B*).

Among DNA repair proteins, Tdp1 appears to be unique in the formation of a phosphohistidyl intermediate with a DNA substrate. Aprataxin also relies on a two-step mechanism of catalytic histidines to remove AMP from 5′-adenylated DNA lesions. However, in this case, the nucleophilic histidine forms a transient covalent bond with the AMP adduct, rather than the adducted DNA, to liberate a free 5′-phosphoryl DNA end (38). It has also been reported that the multifunctional enzyme Tdp2 (also known as TTRAP or EAPII) is more efficient in catalyzing the resolution of 5′-phosphotyrosyl adducts than Tdp1 (39). However, Tdp2 is a member of the exonuclease-endonuclease-phosphatase (or EEP) nuclease family that uses single Mg^{2+}-dependent catalysis to cleave the 5-phosphotyrosine bond and functions in the nonhomologous end joining pathway (40, 41). Thus, Tdp1 and Tdp2 constitute complementary DNA repair activities, with distinct reaction mechanisms (27, 42, 43).

Although the chemistry of DNA transactions catalyzed by topoisomerases and Tdp1 does not require ATP hydrolysis, the downside to the formation of a transient covalent enzyme-DNA intermediate is the potential formation of toxic DNA lesions. This concept has been extensively exploited in the development of microbial and cancer chemotherapeutics, which induce toxicity via the stabilization of enzyme-DNA intermediates (including ciprofloxacin for bacterial DNA gyrase, etoposide for Top2, and CPTs for Top1) (2, 44, 45). In addition, the accumulation of enzyme-DNA intermediates can also result from mutation-induced alterations in DNA cleavage/religation; *e.g.* the self-poisoning Top1 mutants Top1T722A and Top1N726H (46, 47). The best example of a naturally occurring mutation, the Tdp1H493R mutant identified in human SCAN1 patients, is associated with a progressive cerebellar atrophy that presents in the second decade of life (13). Substitution of Arg for His^{gab} enhances the stability of the Tdp1-DNA intermediate *in vitro* and produces a mild toxicity that is recessive to wild type Tdp1 (7, 13, 23, 33).

We previously reported that substituting smaller polar or aliphatic side chains (such as Asn, Glu, Leu, Ala, Ser, or Thr) for the His^{gab} induced more severe cytotoxic phenotypes in yeast (7, 23). Yet, in contrast to results obtained with the yeast SCAN1-like H432R mutant, the use of conventional oligonucleotide-tyrosine substrates did not reveal increased covalent

intermediates *in vitro*. Nevertheless, the Top1-dependent depletion of Tdp1H432N protein in cells was consistent with enhanced H432N-DNA complexes in cells.

The current study extends this concept to demonstrate that alterations in His^{nuc} catalysis can also induce Top1-dependent cytotoxic DNA adducts and that the combination of His^{nuc} and His^{gab} substituents induced an even more severe Top1-independent toxic phenotype. Liu *et al.* (26) previously reported that expression of the His^{nuc} (H182A) mutant in a *tdp1*Δ yeast strain generated a toxic Top1-dependent phenotype and increased cell sensitivity to CPT. However, these studies did not address the catalytic mechanism of this mutant protein. In contrast, our observations suggest that the temporal and spatial coordination of His^{nuc} (His^{182}) and His^{gab} (His^{432}) activities are critical for Tdp1 catalyzed resolution of DNA substrates (Fig. 1*B*). First, expression of H182A (and Tdp1 mutants with other small side chain change substituents of His^{nuc}) induced cell lethality, which was not evident with the introduction of Phe at position 182 (Figs. 2*A* and 5*A*). Our mass spectrometry and mutational analyses of His^{181} (Fig. 6) support the formation of a phosphohistidyl intermediate involving an adjacent His^{181} residue as the probable cause of Tdp1H182A-induced cell lethality (Figs. 2*A* and 3*E*). These data suggest flexibility within the enzyme active site that allows for the formation of His^{181}-DNA intermediates when the His^{nuc} residue is replaced with residues containing a small side chain. Indeed, a His residue immediately N-terminal to His^{nuc} is conserved in the Tdp1 enzyme family. However, in the crystal structures of yeast and human Tdp1, including the apo structure of yeast H182A, His^{181} is facing away from the active site and forms a hydrogen bond with Tyr^{244} (Fig. 7*A*) (7, 22, 23). Rotation of His^{181}, for nucleophilic attack on a DNA adduct, would be easier in the H182A mutant (Fig. 7*B*), because more space is available within the active site, whereas the bulky side chain of Phe at residue 182 would sterically hinder such rotation. Docking or interaction of the Top1-DNA substrate with Tdp1H182A might also induce the rotation of His^{181} and is supported by the predicted ionization state changes of Tdp1 catalytic residues with substrate docking (23). In this context, it is worth noting that lower levels of His^{181} and His^{182} mutant proteins (single or combined with other substitutions) were detected in immunoblots of cell lysates, with a corresponding reduction in the yield of affinity-purified proteins (Fig. 2*C* and data not shown). Because these catalytic residues are located within structurally defined loop domains (Fig. 1*A*), the His^{181} residue may act to stabilize the structure of the protein, thereby facilitating the positioning of the His^{nuc} for efficient catalysis. Indeed, a hydrogen bond between yeast His^{181} and Tyr^{244} (Fig. 7), or the orthologous human His^{262} and Tyr^{330}, suggested in crystal structures of yeast and human Tdp1 (7, 15, 22), may contribute to Tdp1 protein stability in cells.

Another consideration is that the increased distance between the resultant His^{181}-DNA linkage and the His^{gab} residue could preclude effective resolution of the covalent intermediate. Indeed, increased covalent H182A-DNA complexes were observed using oligonucleotide-based substrates *in vitro*, although they were only observed at much higher enzyme concentrations than that observed with the SCAN1-like H432R

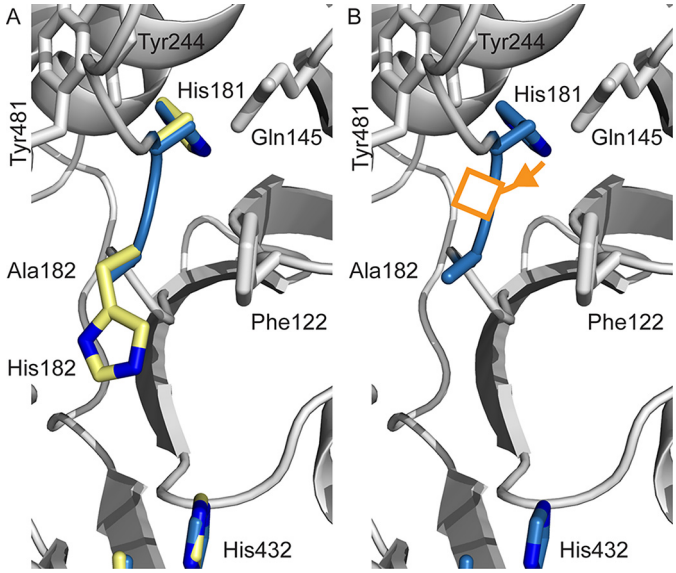

FIGURE 7. **Position of Tdp1 181–182 residues within the catalytic pocket environment.** *A*, overlay of the wild type Tdp1 catalytic histidine residues His^{181}, His^{182}, His^{432} in *yellow* (Protein Data Bank code 1Q32 (7)) and His^{181}, Ala^{182}, and His^{432} residues within the Tdp1H182A crystal structure in *blue* (Protein Data Bank code 3SQ3 (23)). In *gray* is shown the α-carbon backbone trace of Tdp1 protein and surrounding residues that might influence path of rotation. *B*, H182A catalytic pocket focusing on the proposed rotation (*orange arrow*, with the *rectangle* symbolizing end point after rotation) of His^{181} upon docking of the substrate to face the substrate within the active site, which would allow His^{181} to perform a nucleophilic attack. Note the increase distance from His^{432} to His^{182} in *A* and to potential location of His^{181} (after rotation, *orange rectangle*) in *B*.

mutant (Fig. 3, *B*, *D*, and *E*). The low turnover rate (k_{cat}) and 280-fold reduction in second order reaction constant (k_{cat}/K_m) of the H182A mutant, relative to wild type Tdp1, can also be explained by the rotation of His^{181}.

Several lines of evidence also suggest the stabilization of covalent H182A-DNA intermediates in cells. First, the Top1-dependent lethality induced by H182A required the expression of a catalytically active topoisomerase I capable of forming Tdp1 substrates (Fig. 2*B*) and was enhanced by CPT targeting of topoisomerase I. Second, the lethal phenotype induced by H182A expression was recessive to wild type Tdp1, consistent with the resolution of adducted DNA by the wild type enzyme. Together, these data support the concept that the degree of Tdp1-induced toxicity is dependent upon the levels of the Top1-DNA substrate and their conversion to Tdp1-DNA intermediates. Similar results were obtained with H432N (7); however, only the double H182A,H432N mutant exhibited a Topoisomerase I-independent lethality, which was only partially suppressed by wild type Tdp1. These findings suggest that other, spontaneous DNA adducts also serve as endogenous substrates for Tdp1-mediated repair.

Our biochemical characterizations and studies in yeast strains deleted for the Rad9 DNA damage checkpoint (*rad9*Δ cells) further suggest that the DNA adducts induced by Tdp1H182A and H432N are distinct from those induced by the SCAN1-like H432R mutant enzyme. Notably, *rad9*Δ induced a >3-log drop in the viability of CPT-treated cells expressing either the H182A or H432N mutant enzyme, but not the H432R mutant (Fig. 4). These data indicate that alterations in Tdp1H182A or H432N catalysis suffice to induce DNA lesions

that activate the Rad9 DNA damage checkpoint. Given the recessive nature of the Top1-dependent lethality of these mutant enzymes, we posit that such adducted DNA likely involves covalent mutant Tdp1-DNA complexes. If we consider the kinetics of Tdp1-DNA intermediate formation using the oligonucleotide substrate, no intermediates are detected with wild type Tdp1. With the H432R mutant enzyme, reaction intermediates are detected; however, they accumulate prior to detectable product, suggesting a delay in covalent complex resolution. If the reaction intermediate is buried within the active site of Tdp1H432R, possibly because of the tighter DNA binding suggested by the surface charge topography of the apo crystal structure (23), then the sequestration of this DNA adduct might prevent activation of the Rad9 DNA damage checkpoint, even in the presence of CPT.

In contrast, Tdp1H182A-DNA intermediates are detected at 10–25-fold higher concentrations than those needed for substrate conversion to product, which suggests the inability of H182A or H432N mutant enzymes to resolve the covalent intermediate. Thus, the increased flexibility or spatial distortion of the Tdp1 active site, which impairs the resolution of the reaction intermediates, may also trigger alternative Rad9-dependent DNA repair pathways to induce even more toxic DNA lesions. These results are reminiscent of CPT poisoning of Top1-DNA complexes or of the self-poisoning mutants Top1N722H and Top1T718A, which accumulate Top1-DNA complexes via distinct defects in catalysis (46, 47). Top1N722H exhibits an enhanced rate of DNA cleavage (formation of the covalent Top1-DNA complex), and Top1T718A displays a reduced religation rate (slower resolution of the covalent intermediate), whereas the double mutant is even more toxic than either single mutant enzyme. The same attributes may be extended to the H182A and H432N Tdp1 mutants, where double mutants are more toxic than the single mutants (Figs. 2*A* and 4) and induces a unique Top1-independent lethality that is not suppressed by the Rad9 checkpoint or wild type Tdp1 (Figs. 2 and 4). Taken together, our findings demonstrate distinct mechanisms of cytotoxicity are induced by mutation of the catalytic His^{nuc} or His^{gab} residues in Tdp1. The conservation of Tdp1 enzyme-induced lethality is supported by the similar dysregulation of human and yeast SCAN1-associated His^{gab} to Arg mutants, including the increased half-life of the covalent reaction intermediate *in vitro* and enhanced cell sensitivity to CPT (7, 16, 23, 33). Moreover, preliminary studies of mammalian cells expressing human hTdp1H493N and hTdp1H263A mutants (analogous to yeast Tdp1H432N and Tdp1H182A, respectively, (23)) indicate the induction of a similar cytotoxic phenotype.[4] Thus, the mechanisms of yeast Tdp1 enzyme dysregulation, described in these studies, also appear to be a feature of human Tdp1. Moreover, these observations support the concept that the targeting of Tdp1 to develop small molecules that poison the enzyme by increasing the stability of Tdp1-DNA intermediates represents a novel chemotherapeutic strategy.

[4] S. Cuya, E. Comeaux, and R. van Waardenburg, unpublished data.

Acknowledgments—We thank Melissa Gessner and Keke Pounds for technical assistance, Katie Jo Glowacki for help with analyzing enzyme kinetics using VisualEnzymics-IGOR PRO 6, and Dr. Charles Falany for discussing enzyme kinetics.

REFERENCES

1. Yang, S. W., Burgin, A. B., Jr., Huizenga, B. N., Robertson, C. A., Yao, K. C., and Nash, H. A. (1996) A eukaryotic enzyme that can disjoin dead-end covalent complexes between DNA and type I topoisomerases. *Proc. Natl. Acad. Sci. U.S.A.* **93,** 11534–11539
2. Hsiang, Y. H., Hertzberg, R., Hecht, S., and Liu, L. F. (1985) Camptothecin induces protein-linked DNA breaks via mammalian DNA topoisomerase I. *J. Biol. Chem.* **260,** 14873–14878
3. Hsiang, Y. H., Lihou, M. G., and Liu, L. F. (1989) Arrest of replication forks by drug-stabilized topoisomerase I-DNA cleavable complexes as a mechanism of cell killing by camptothecin. *Cancer Res.* **49,** 5077–5082
4. Pommier, Y., Leo, E., Zhang, H., and Marchand, C. (2010) DNA topoisomerases and their poisoning by anticancer and antibacterial drugs. *Chem. Biol.* **17,** 421–433
5. Schoeffler, A. J., and Berger, J. M. (2008) DNA topoisomerases: harnessing and constraining energy to govern chromosome topology. *Q. Rev. Biophys.* **41,** 41–101
6. Wang, J. C. (2002) Cellular roles of DNA topoisomerases: a molecular perspective. *Nat. Rev. Mol. Cell Biol.* **3,** 430–440
7. He, X., van Waardenburg, R. C., Babaoglu, K., Price, A. C., Nitiss, K. C., Nitiss, J. L., Bjornsti, M. A., and White, S. W. (2007) Mutation of a conserved active site residue converts tyrosyl-DNA phosphodiesterase I into a DNA topoisomerase I-dependent poison. *J. Mol. Biol.* **372,** 1070–1081
8. Huang, S. Y., Murai, J., Dalla Rosa, I., Dexheimer, T. S., Naumova, A., Gmeiner, W. H., and Pommier, Y. (2013) TDP1 repairs nuclear and mitochondrial DNA damage induced by chain-terminating anticancer and antiviral nucleoside analogs. *Nucleic Acids Res.* **41,** 7793–7803
9. Inamdar, K. V., Pouliot, J. J., Zhou, T., Lees-Miller, S. P., Rasouli-Nia, A., and Povirk, L. F. (2002) Conversion of phosphoglycolate to phosphate termini on 3′ overhangs of DNA double strand breaks by the human tyrosyl-DNA phosphodiesterase hTdp1. *J. Biol. Chem.* **277,** 27162–27168
10. Interthal, H., Chen, H. J., and Champoux, J. J. (2005) Human Tdp1 cleaves a broad spectrum of substrates, including phosphoamide linkages. *J. Biol. Chem.* **280,** 36518–36528
11. Lebedeva, N. A., Rechkunova, N. I., and Lavrik, O. I. (2011) AP-site cleavage activity of tyrosyl-DNA phosphodiesterase 1. *FEBS Lett.* **585,** 683–686
12. Raymond, A. C., Rideout, M. C., Staker, B., Hjerrild, K., and Burgin, A. B., Jr. (2004) Analysis of human tyrosyl-DNA phosphodiesterase I catalytic residues. *J. Mol. Biol.* **338,** 895–906
13. Takashima, H., Boerkoel, C. F., John, J., Saifi, G. M., Salih, M. A., Armstrong, D., Mao, Y., Quiocho, F. A., Roa, B. B., Nakagawa, M., Stockton, D. W., and Lupski, J. R. (2002) Mutation of TDP1, encoding a topoisomerase I-dependent DNA damage repair enzyme, in spinocerebellar ataxia with axonal neuropathy. *Nat. Genet.* **32,** 267–272
14. Davies, D. R., Interthal, H., Champoux, J. J., and Hol, W. G. (2002) Insights into substrate binding and catalytic mechanism of human tyrosyl-DNA phosphodiesterase (Tdp1) from vanadate and tungstate-inhibited structures. *J. Mol. Biol.* **324,** 917–932
15. Davies, D. R., Interthal, H., Champoux, J. J., and Hol, W. G. (2002) The crystal structure of human tyrosyl-DNA phosphodiesterase, Tdp1. *Structure* **10,** 237–248
16. Interthal, H., Pouliot, J. J., and Champoux, J. J. (2001) The tyrosyl-DNA phosphodiesterase Tdp1 is a member of the phospholipase D superfamily. *Proc. Natl. Acad. Sci. U.S.A.* **98,** 12009–12014
17. Pouliot, J. J., Yao, K. C., Robertson, C. A., and Nash, H. A. (1999) Yeast gene for a Tyr-DNA phosphodiesterase that repairs topoisomerase I complexes. *Science* **286,** 552–555
18. Caldecott, K. W. (2003) DNA single-strand break repair and spinocerebellar ataxia. *Cell* **112,** 7–10
19. Das, B. B., Antony, S., Gupta, S., Dexheimer, T. S., Redon, C. E., Garfield, S., Shiloh, Y., and Pommier, Y. (2009) Optimal function of the DNA repair

enzyme TDP1 requires its phosphorylation by ATM and/or DNA-PK. *EMBO J.* **28,** 3667–3680
20. Karimi-Busheri, F., Daly, G., Robins, P., Canas, B., Pappin, D. J., Sgouros, J., Miller, G. G., Fakhrai, H., Davis, E. M., Le Beau, M. M., and Weinfeld, M. (1999) Molecular characterization of a human DNA kinase. *J. Biol. Chem.* **274,** 24187–24194
21. Whitehouse, C. J., Taylor, R. M., Thistlethwaite, A., Zhang, H., Karimi-Busheri, F., Lasko, D. D., Weinfeld, M., and Caldecott, K. W. (2001) XRCC1 stimulates human polynucleotide kinase activity at damaged DNA termini and accelerates DNA single-strand break repair. *Cell* **104,** 107–117
22. Davies, D. R., Interthal, H., Champoux, J. J., and Hol, W. G. (2003) Crystal structure of a transition state mimic for Tdp1 assembled from vanadate, DNA, and a topoisomerase I-derived peptide. *Chem. Biol.* **10,** 139–147
23. Gajewski, S., Comeaux, E. Q., Jafari, N., Bharatham, N., Bashford, D., White, S. W., and van Waardenburg, R. C. (2012) Analysis of the active-site mechanism of tyrosyl-DNA phosphodiesterase I: a member of the phospholipase D superfamily. *J. Mol. Biol.* **415,** 741–758
24. El-Khamisy, S. F., Saifi, G. M., Weinfeld, M., Johansson, F., Helleday, T., Lupski, J. R., and Caldecott, K. W. (2005) Defective DNA single-strand break repair in spinocerebellar ataxia with axonal neuropathy-1. *Nature* **434,** 108–113
25. Zhou, T., Lee, J. W., Tatavarthi, H., Lupski, J. R., Valerie, K., and Povirk, L. F. (2005) Deficiency in 3′-phosphoglycolate processing in human cells with a hereditary mutation in tyrosyl-DNA phosphodiesterase (TDP1). *Nucleic Acids Res.* **33,** 289–297
26. Liu, C., Pouliot, J. J., and Nash, H. A. (2004) The role of TDP1 from budding yeast in the repair of DNA damage. *DNA Repair* **3,** 593–601
27. Nitiss, K. C., Malik, M., He, X., White, S. W., and Nitiss, J. L. (2006) Tyrosyl-DNA phosphodiesterase (Tdp1) participates in the repair of Top2-mediated DNA damage. *Proc. Natl. Acad. Sci. U.S.A.* **103,** 8953–8958
28. Kauh, E. A., and Bjornsti, M. A. (1995) SCT1 mutants suppress the camptothecin sensitivity of yeast cells expressing wild-type DNA topoisomerase I. *Proc. Natl. Acad. Sci. U.S.A.* **92,** 6299–6303
29. Sauer, B., and Henderson, N. (1990) Targeted insertion of exogenous DNA into the eukaryotic genome by the Cre recombinase. *New Biol.* **2,** 441–449
30. Akada, R., Kitagawa, T., Kaneko, S., Toyonaga, D., Ito, S., Kakihara, Y., Hoshida, H., Morimura, S., Kondo, A., and Kida, K. (2006) PCR-mediated seamless gene deletion and marker recycling in *Saccharomyces cerevisiae*. *Yeast* **23,** 399–405
31. Megonigal, M. D., Fertala, J., and Bjornsti, M. A. (1997) Alterations in the catalytic activity of yeast DNA topoisomerase I result in cell cycle arrest and cell death. *J. Biol. Chem.* **272,** 12801–12808
32. Lynn, R. M., Bjornsti, M. A., Caron, P. R., and Wang, J. C. (1989) Peptide sequencing and site-directed mutagenesis identify tyrosine-727 as the active site tyrosine of *Saccharomyces cerevisiae* DNA topoisomerase I. *Proc. Natl. Acad. Sci. U.S.A.* **86,** 3559–3563
33. Interthal, H., Chen, H. J., Kehl-Fie, T. E., Zotzmann, J., Leppard, J. B., and Champoux, J. J. (2005) SCAN1 mutant Tdp1 accumulates the enzyme-DNA intermediate and causes camptothecin hypersensitivity. *EMBO J.* **24,** 2224–2233
34. Pouliot, J. J., Robertson, C. A., and Nash, H. A. (2001) Pathways for repair of topoisomerase I covalent complexes in *Saccharomyces cerevisiae*. *Genes Cells* **6,** 677–687
35. Solimini, N. L., Xu, Q., Mermel, C. H., Liang, A. C., Schlabach, M. R., Luo, J., Burrows, A. E., Anselmo, A. N., Bredemeyer, A. L., Li, M. Z., Beroukhim, R., Meyerson, M., and Elledge, S. J. (2012) Recurrent hemizygous deletions in cancers may optimize proliferative potential. *Science* **337,** 104–109
36. Ciccia, A., and Elledge, S. J. (2010) The DNA damage response: making it safe to play with knives. *Mol. Cell* **40,** 179–204
37. Yang, W. (2010) Topoisomerases and site-specific recombinases: similarities in structure and mechanism. *Crit. Rev. Biochem. Mol. Biol.* **45,** 520–534
38. Tumbale, P., Appel, C. D., Kraehenbuehl, R., Robertson, P. D., Williams, J. S., Krahn, J., Ahel, I., and Williams, R. S. (2011) Structure of an aprataxin-DNA complex with insights into AOA1 neurodegenerative disease. *Nat. Struct. Mol. Biol.* **18,** 1189–1195
39. Cortes Ledesma, F., El Khamisy, S. F., Zuma, M. C., Osborn, K., and Caldecott, K. W. (2009) A human 5′-tyrosyl DNA phosphodiesterase that repairs topoisomerase-mediated DNA damage. *Nature* **461,** 674–678
40. Schellenberg, M. J., Appel, C. D., Adhikari, S., Robertson, P. D., Ramsden, D. A., and Williams, R. S. (2012) Mechanism of repair of 5′-topoisomerase II-DNA adducts by mammalian tyrosyl-DNA phosphodiesterase 2. *Nat. Struct. Mol. Biol.* **19,** 1363–1371
41. Shi, K., Kurahashi, K., Gao, R., Tsutakawa, S. E., Tainer, J. A., Pommier, Y., and Aihara, H. (2012) Structural basis for recognition of 5′-phosphotyrosine adducts by Tdp2. *Nat. Struct. Mol. Biol.* **19,** 1372–1377
42. Murai, J., Huang, S. Y., Das, B. B., Dexheimer, T. S., Takeda, S., and Pommier, Y. (2012) Tyrosyl-DNA phosphodiesterase 1 (TDP1) repairs DNA damage induced by topoisomerases I and II and base alkylation in vertebrate cells. *J. Biol. Chem.* **287,** 12848–12857
43. Zeng, Z., Cortés-Ledesma, F., El Khamisy, S. F., and Caldecott, K. W. (2011) TDP2/TTRAP is the major 5′-tyrosyl DNA phosphodiesterase activity in vertebrate cells and is critical for cellular resistance to topoisomerase II-induced DNA damage. *J. Biol. Chem.* **286,** 403–409
44. Chen, G. L., Yang, L., Rowe, T. C., Halligan, B. D., Tewey, K. M., and Liu, L. F. (1984) Nonintercalative antitumor drugs interfere with the breakage-reunion reaction of mammalian DNA topoisomerase II. *J. Biol. Chem.* **259,** 13560–13566
45. Sioud, M., and Forterre, P. (1989) Ciprofloxacin and etoposide (VP16) produce a similar pattern of DNA cleavage in a plasmid of an archaebacterium. *Biochemistry* **28,** 3638–3641
46. Colley, W. C., van der Merwe, M., Vance, J. R., Burgin, A. B., Jr., and Bjornsti, M. A. (2004) Substitution of conserved residues within the active site alters the cleavage religation equilibrium of DNA topoisomerase I. *J. Biol. Chem.* **279,** 54069–54078
47. Fertala, J., Vance, J. R., Pourquier, P., Pommier, Y., and Bjornsti, M. A. (2000) Substitutions of Asn-726 in the active site of yeast DNA topoisomerase I define novel mechanisms of stabilizing the covalent enzyme-DNA intermediate. *J. Biol. Chem.* **275,** 15246–15253